Effect of crosslinking fraction, hardener functionality and topological quality on stress recovery of thermoset shape memory polymers: a coarse-grained molecular dynamics study

To cite this article: Pouria Nourian *et al* 2023 *Smart Mater. Struct.* **32** 115001

IOP Publishing Smart Materials and Structures
Smart Mater. Struct. **32** (2023) 115001 (9pp) https://doi.org/10.1088/1361-665X/acfa7d

Effect of crosslinking fraction, hardener functionality and topological quality on stress recovery of thermoset shape memory polymers: a coarse-grained molecular dynamics study

Pouria Nourian, Collin D Wick and Andrew J Peters*

College of Engineering and Science, Louisiana Tech University, Ruston, LA 71270, United States of America

E-mail: apeters@latech.edu

Received 19 April 2023, revised 28 August 2023
Accepted for publication 17 September 2023
Published 26 September 2023

Abstract

We analyzed the effects of crosslinking fraction and number of functional sites per hardener molecule on the stress recovery and topology of thermoset shape memory polymers (TSMPs) via coarse-grained molecular dynamics simulations. After systematically varying the quality of the crosslinked network by manipulating the number of unique epoxies reacted with each hardener, we found that two fingerprints correlate well with stress recovery of TSMPs. These fingerprints are the fraction of epoxy molecules connected to two distinct hardener molecules, and the fraction of molecules that are part of the largest or main network in the system. Their product can be used as a topological score (S_{topo}) to quantify the topological feature of the network. When analyzing stress recovery as a function of S_{topo}, we found a strong correlation between S_{topo} and recovery stress. Moreover, we observed that while a higher crosslinking fraction did frequently lead to a higher stress recovery, many exceptions existed. High functionality hardeners tend to exhibit higher stress recovery at similar S_{topo}, especially at high (>0.65) S_{topo}. These results suggest that increasing the number of functional sites per hardener molecule combined with improving the topology of the network with a method such as semi batch monomer addition can lead to an improvement in the stress recovery of TSMPs.

Supplementary material for this article is available online

Keywords: thermoset shape meory polymer, molecular dynamics, simulation, coarse-grained, crosslinking, topological, recovery stress

(Some figures may appear in colour only in the online journal)

1. Introduction

Shape memory polymers (SMPs) are materials capable of remembering and reverting to their permanent memorized shape from a deformed state in response to thermal or non-thermal stimuli such as temperature, light, moisture, or pH. Such a feature, in addition to other desirable properties such as chemical stability, potential for biodegradability, relative ease of processability, and low costs of production, have been proven to be beneficial in many industries [1, 2]. SMPs can be used as minimally invasive medical devices [3–9] or as drug

* Author to whom any correspondence should be addressed.

delivery vehicles [10, 11] in the biomedical industry. They can be used for fabricating deployable or morphing structures in the aerospace industry [12–15], or used for controlling the surface morphology when making composite electronics [16–19].

The temporary shape can be induced in SMPs via a process known as 'hot programming', where the material is prestrained at temperatures sufficiently higher than its glass transition temperature (T_g), then cooled to a temperature below T_g while constrained. When the constrain is removed at low temperatures, the material is fixed with a temporary shape, and when it is heated to a temperature above its T_g, the material recovers to its original shape. The SMPs' ability to recover their original shape is quantified by the shape recovery ratio, which is a measure of how much of the original shape is recovered, and stress recovery, which is the stress that the material exerts while it is recovering its original shape.

One of the main issues impeding the widespread use of SMPs for the aforementioned applications, especially in cases where high performance is required, is the low-stress recovery of the current generation of SMPs [20], which prohibits the material to support heavier samples [21]. One of the main approaches to enhancing the properties of SMPs is through the incorporation of nanofillers such as carbon nanotubes [22–24], particulates [25, 26], and fibers [12, 27, 28] in the polymer matrix. Such an approach, while successful at improving the recovery stress (σ_r), can lead to a noticeable loss of shape memory. Naturally, approaches that improve aspects of the shape memory property without any tradeoff will be more desirable.

One such approach would be improving the topology of the shape memory polymer networks. Inspired by previous studies on the interplay between the topology and the mechanical properties of polymer networks, such as the effect of cyclic defects, i.e., elastically inactive primary loops [29–34]) and secondary loops [35–37] on the elastic and storage moduli of these networks [38–42], we recently studied the effect of topology on the shape memory properties of the thermoset shape memory polymers (TSMPs) [43]. We discovered statistically significant correlations among the stress recovery, recovery ratio, rubbery elastic modulus, and the fraction of hardener molecules that have formed the maximum number of bonds with distinct epoxy molecules. Such hardener molecules are the building blocks of a perfect network, and thus, the closer a network to perfection is, the better its shape memory properties are. However, in our previous study, the scope of our work was limited to systems with a single crosslinking fraction, and only one type of hardener molecule.

In this work, we aim to expand upon our previous work to investigate the relationship between the topology and the shape memory properties of TSMPs more broadly by taking into account the effect of various crosslinking fractions and the number of functional/reaction sites per hardener molecules (i.e. hardener functionality). Our goal is not to closely follow the experimental procedures used to create these networks, but rather, create a set of systems with extreme variations in topology (through implementing irregular conditions and assumptions) and further investigate the interplay between topology and the shape memory properties, and the limits of the effect of topology on such properties. We use coarse-grained molecular dynamics simulations to forgo the effect of chemistry on the properties of simulated systems and instead focus solely on the topological effect. Moreover, since studying the topology comprehensively requires simulating many systems, a coarse-grained model allows us to do so using only a fraction of the computational resources required when using atomistically detailed models. Finally, we want to identify topology-related quantities that have statistically significant correlations with the shape memory properties of the TSMPs. These topological 'fingerprints' can then be used in conjunction with chemical fingerprints [44] to train machine-learning algorithms that can be used to identify hardener–epoxy pairs that would yield high-performance TSMPs.

In the following sections, we will provide a detailed explanation of the model and simulations we used. Next, we will present the results of our simulations, including any statistically significant correlations found between recovery stress and various topological properties. Finally, we will discuss the significance of our findings and their physical interpretation.

2. Methodology

2.1. Model details

A coarse-grained model is used to represent the hardeners and epoxies. The epoxies are modeled as a chain with 3 beads, with a nonreactive middle bead and two reactive end beads. Four different types of hardener molecules are used with 3, 4, 5 and 6 reactive beads (referred to as f_3, f_4, f_5 and f_6 hardeners, respectively). Each hardener molecule is modeled as having one non-reactive bead in the center (figure 1) with the reactive beads each bonded directly to the nonreactive core bead.

The non-bonded interactions between all the beads were represented using the Weeks–Chandler–Anderson (WCA) potential [45], as follows:

$$U_{\mathrm{WCA}}(r) = 4\varepsilon\left[\left(\frac{\sigma}{r}\right)^{12} - \left(\frac{\sigma}{r}\right)^{6}\right] \quad r < 2^{\frac{1}{6}}\sigma$$
$$U_{\mathrm{WCA}} = 0 \quad r \geqslant 2^{\frac{1}{6}}\sigma \qquad (1)$$

where r is the inter-particle distance, ε is the interaction strength, and σ is the bead diameter. The WCA potential has demonstrated versatility in modeling the behavior of polymer melts and networks [46–49]. The potential parameters, σ and ϵ, and the mass of individual particles, m are set equal to 1. The rest of the quantities are presented in the reduced units as follows: Reduced time: $\tau^* = \frac{\tau}{\sqrt{\frac{m\sigma^2}{\epsilon}}}$, reduced temperature: $T^* = \frac{k_B T}{\epsilon}$, reduced distance: $r^* = \frac{r}{\sigma}$, reduced pressure: $p^* = \frac{p}{\frac{\epsilon}{\sigma^3}}$, etc. The bonded interactions were represented using the bead-spring model, where consecutive beads are connected by finitely extensible nonlinearly elastic (FENE) springs [46], as follows:

$$U_{\mathrm{FENE}}(r) = -0.5QR_0{}^2 \ln\left(1 - \left(\frac{r}{R_0}\right)\right) \qquad (2)$$

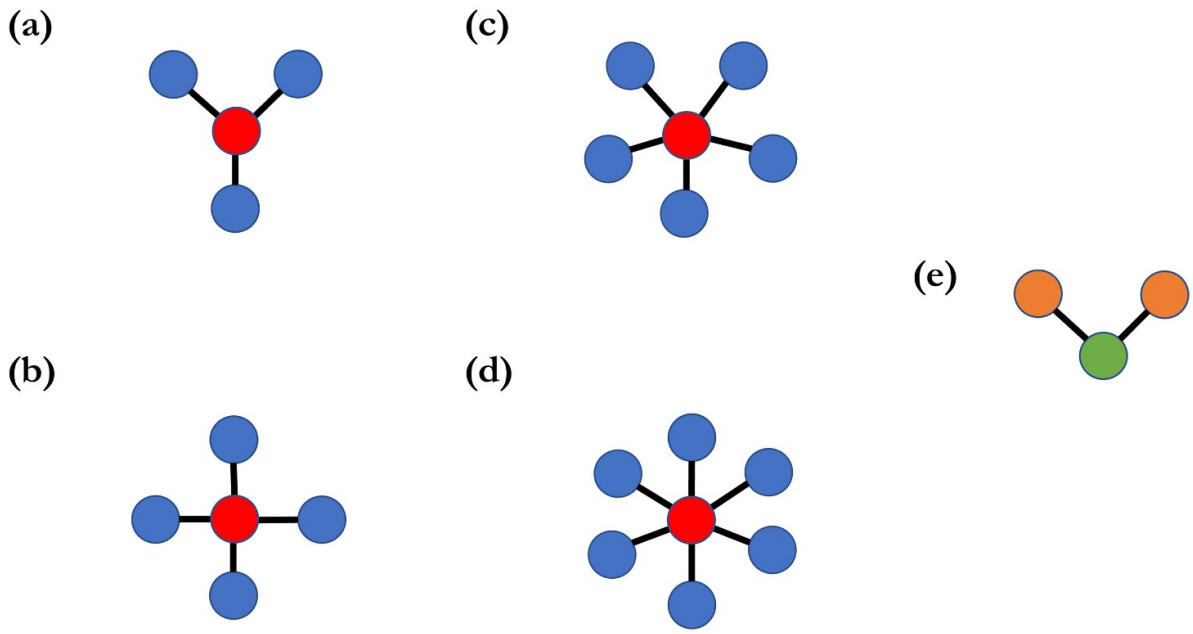

Figure 1. Schematics of a hardener molecule with (a) 3 reactive sites (f_3), (b) 4 reactive sites (f_4), (c) 5 reactive sites (f_5), (d) 6 reactive sites (f_6), and (e) an epoxy molecule. The blue and red colors represent the reactive and non-reactive beads of the hardener molecule, respectively. The green and orange colors represent the reactive and non-reactive beads of the epoxy molecule, respectively.

where r is the inter-particle distance, Q is the spring constant, and R_0 is the maximum allowable extension. Here, values of $Q = 30$ and $R_0 = 1.5$ were used.

2.2. Simulation details

All the simulations were conducted in the absence of solvent, with the periodic boundary conditions being imposed on the cubic simulation boxes in all three directions. Moreover, the LAMMPS software package [50] was used to conduct all the simulations in the constant number of atoms, pressure, and temperature (NPT) ensemble. A timestep of 0.003 was used in the simulations. Nose-Hoover thermostats and barostat [51, 52] were utilized, and the damping constants for temperature and pressure control were set to be 100 times and 1000 times the timestep, respectively. Pressures and temperatures are specified below.

2.3. Crosslinking and bond relaxation

Initial simulation boxes were prepared by randomly placing 2000 hardener molecules and an appropriate number of epoxy molecules to maintain a stoichiometric ratio (3000 for f_3 systems, 4000 for f_4 systems, 5000 for f_5 systems and 6000 for f_6 systems) in a cubic box with an initial length ranging from 35 to 50 using the Polymatic software [53]. A custom Python script was used to create bonds between the reactive beads of the epoxies and hardeners by randomly selecting hardener and epoxy molecules for reaction. As mentioned earlier, we previously found that the fraction of hardener molecules that have formed the maximum number of bonds possible with distinct epoxy molecules can be used as a descriptor of the topology, and the higher this fraction is, the better the quality of the topology is [43]. Based on this fact, in order to obtain systems with a variety of topologies, we manipulated the topology via imposing a condition on the systems during the preparation phase: each hardener molecule participating in the reaction was ensured to have the maximum number of bonds possible formed with other epoxies. For instance, all hardeners in the f_3 system had 3 bonds, all hardeners in the f_4 system had 4 bonds, etc. Using this approach, 25 systems were created for each of the hardener types. In each set, systems indexed 1–5 had a crosslinking fraction (i.e. the ratio of number of bonds formed between hardeners and epoxies to the maximum possible number of bonds between those molecule types) of 0.5, systems 6–10 had a crosslinking fraction of 0.6, systems 11–15 had a crosslinking fraction of 0.7, systems 16–20 had a crosslinking fraction of 0.8, and systems 21–25 had a crosslinking fraction of 0.9. Furthermore, each system was required to have a minimum number of maximally-distinctly-reacted hardener molecules. A maximally-distinctly-reacted hardener molecule has all sites reacted with a different epoxy. This lower limit was set to be 20% of the total hardener molecules in the first system in each set, 25% for the second system, 30% for the third system, 35% for the fourth system, and 40% for the fifth system. This method created systems with the same crosslinking fraction and hardener functionality (i.e. number of functional sites per molecule) but with significantly different topologies. While the systems created using this approach may not be feasible using current experimental methods, their distribution of topological quality can be utilized to study the limits of the effect of topology on the shape memory properties. A bond between an epoxy–hardener reactive pair was formed when the distance between the two reactive sites was ten or less. In

order to shorten the bonds with a length greater than the maximum allowable extension of 1.5 used in the FENE potential, we used a stepwise bond relaxation approach to shorten those abnormally long bonds, as follows: A harmonic potential for the bonds formed during the crosslinking procedure:

$$U_{\text{Harmonic}}(r) = K(r - r_0)^2 \tag{3}$$

where K is the bond spring constant, r is the bond length and r_0 is the bond equilibrium length. The FENE potential was used to represent the rest of the bonds. At each step of the relaxation procedure, the systems were relaxed in the NPT ensemble at a temperature of 1 and a pressure of 4 for a duration of 10 000 simulation steps. In each consecutive step, the bond spring constant was increased, and the bond equilibrium length was decreased. This process was repeated for a total of ten steps. The initial and final bond spring constants used were 0.3 and 30, respectively, and the initial and final bond equilibrium lengths used were 30 and 1.5, respectively. Once the stepwise bond relaxation procedure was completed, the systems were equilibrated in the NPT ensemble a temperature of 1 and a pressure of 4 for a duration of 1000 000 simulation steps, where the FENE potential was applied to all the bonds in the system. Visual representations of systems with two different crosslinking fractions can be found in the supplementary information.

2.4. Programming

The determination of programming and recovery stress was carried out in the same manner as previously described [43]. The systems were compressed to 50% overall compression and held at that compression for 1000 000 timesteps. Then, the systems were cooled to a temperature of 0.05 (well below the glass transition temperature) and allowed to relax. After heating back to the original temperature at 50% compression, the system was further relaxed, and the recovery stress was measured. This process was repeated in all three dimensions independently, and the results were then averaged.

3. Results and discussion

3.1. Correlations between stress recovery and topological fingerprints

A total of 100 systems with four different hardener molecules and five different crosslinking fractions were created. In each system, a series of topological fingerprints were calculated as follows:

- H_f, the fraction of hardener molecules connected to the maximum number of distinct epoxy molecules, where f is the number of reactive beads per hardener molecule.
- E_2, the fraction of epoxy molecules bonded to two distinct hardener molecules.
- F_{max}, the fraction of total molecules in the largest network formed in the system.

Details regarding the calculation of the fingerprints from simulation data can be found in supplementary information. The first fingerprint, H_f, is based upon our previous work, where we showed that each hardener with the maximum number of reactions with distinct epoxy molecules can be thought of as a building block of a perfect network. However, such a hardener molecule may or may not be connected to the largest network in the system. In this case, one could hypothesize that such molecules will not be significant contributors to the shape memory properties of the material. Therefore, we include the other two fingerprints, E_2 and F_{max}, to complement H_f. In a perfect network, all hardener molecules are connected via two-distinctly-reacted epoxy molecules, and all are part of the same network. Thus, E_2 and F_{max} are also measures of how perfect a network is. One could also view these three fingerprints as a measure of how a network deviates from a perfect network, since in a perfect network, all these fingerprints have a value of 1. Thus, we would expect these fingerprints to have statistically significant correlations with the shape memory properties of the networks. These quantities, along with the stress recovery (σ_r), are presented in figure 2 for all the systems. A detailed description regarding the calculation of these fingerprints is presented in the Supplementary Information.

As observed in figure 2, all three fingerprints and the stress recovery follow the same trend: a higher value of any of these fingerprints corresponds to a higher stress recovery. To further evaluate the relation between these three fingerprints and σ_r, we calculated the Pearson correlation coefficients and their statistical significance between H_f, E_2, F_{max}, and σ_r. These results are presented in table 1.

We observe that while all the correlations between H_f, E_2, F_{max} (as expected, since they describe the topology of the system which is the only difference between simulations with the same hardener functionality), and σ_r are statistically significant (i.e. their corresponding p-values is less than 0.05), the correlation coefficients corresponding to E_2 and F_{max} are significantly greater—and their p-values significantly smaller—than those corresponding to H_4, H_5, and H_6. This means that while all three fingerprints encompass a great amount of information about the topology in f_3 systems, E_2 and F_{max} are better fingerprints in f_4, f_5, and f_6 systems.

These results validate our initial hypothesis that the H_f fingerprint does not in general contain all the information about the topology of the system and demonstrate that E_2 and F_{max} are better fingerprints. This can be further improved upon by using what we call the 'topological score' or S_{topo} and defined by $S_{topo} = E_2 F_{max}$. F_{max} scales the score by the number of molecules able to contribute to the network, and E_2 scales the score by the number of effective connections between those available molecules. A network with a large number of primary loops will have a high F_{max} but a low E_2, and a system where a large number of molecules are not part of the main network will have a low F_{max} even if it has a high E_2. In both cases a poor stress recovery would be expected. We plot the stress recovery of the systems studied versus their topological scores in figure 3.

As observed in figure 3, a higher crosslinking fraction (CF) allows for higher S_{topo} and subsequently higher σ_r in line with

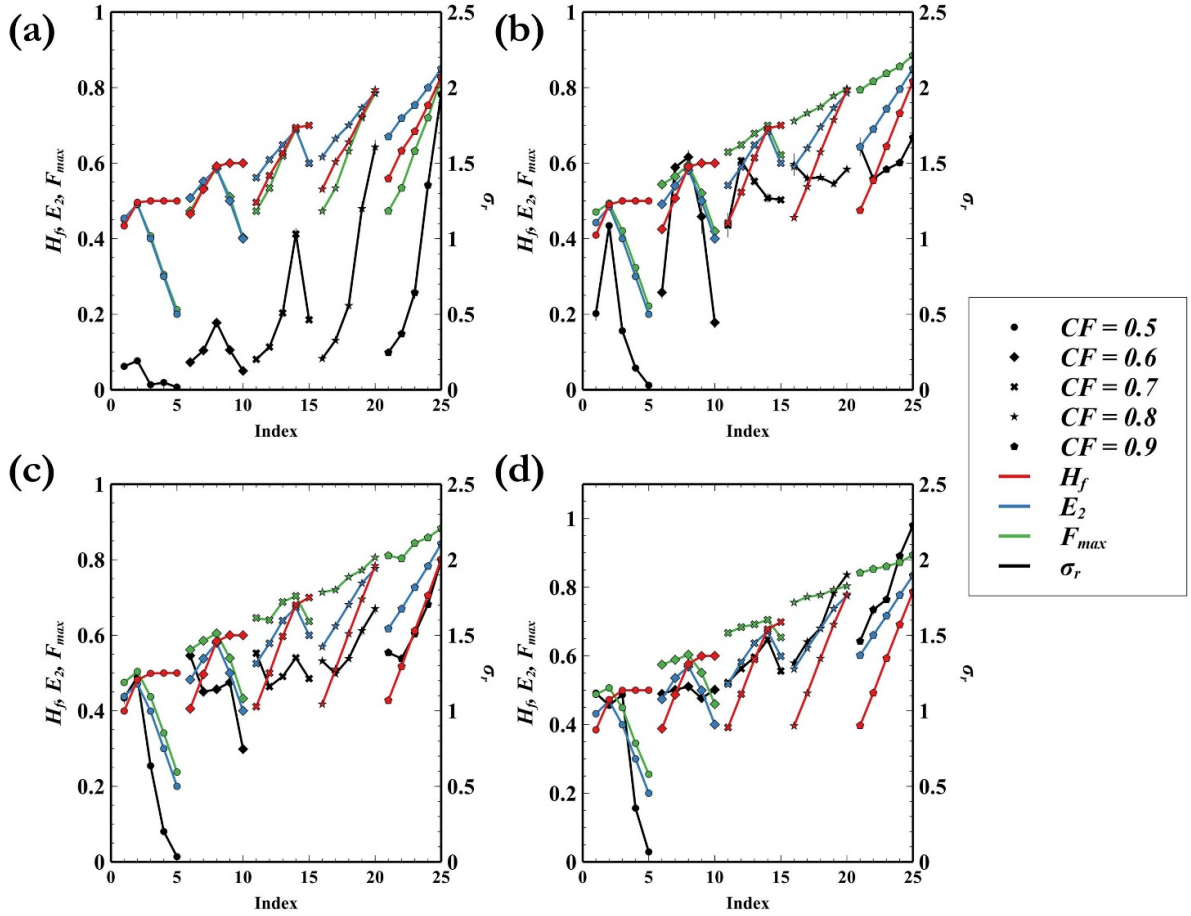

Figure 2. The fraction of maximally distinctly reacted hardener molecules (H_f, red), two-distinctly reacted epoxy molecules (E_2, blue), fractional maximum size of the main network (F_{max}, green), and the stress recovery (σ_r, purple) vs. the system index (numbered from 1 to 25) for (a) f_3 systems, (b) f_4 systems, (c) f_5 systems, and (d) f_6 systems. Systems indexed 1–5 have a crosslinking fraction of 0.5 (circles), systems 6–10 have a crosslinking fraction of 0.6 (diamonds), systems 11–15 have a crosslinking fraction of 0.7 (crosses), systems 16–20 have a crosslinking fraction of 0.8 (stars), and systems 21–25 have a crosslinking fraction of 0.9 (pentagons).

our expectations. However, it can be observed that quite a few instances exist where systems with a lower *CF* have achieved a higher stress recovery. The crosslinking fraction sets the upper limit of all the three discussed fingerprints (H_f, E_2 and F_{max}), as each of these fingerprints can attain a maximum value equal to *CF*, and thus, the maximum value for the topological score will be CF^2. A system with a higher *CF* has a higher potential for having better shape memory properties, but a higher *CF* alone does not ensure better properties, as illustrated in figure 3, where certain systems with lower *CF* exhibit superior stress recovery compared to systems with higher *CF*. The crosslinking fraction can be thought of as the budget for creating a network, and the topological score will then represent how well that budget is spent. A system made with a low, albeit better-spent budget, or in other words, a system with a lower *CF* but higher S_{topo}, can have better shape memory properties than a system with a higher *CF* and lower S_{topo}.

The *CF* dictates the quantity of epoxy–hardener bonds present within the system, whereas S_{topo} gauges the similarity of the bond distribution to that of an ideal network. A network may have a higher bond count, but that does not necessarily mean that the bond distribution resembles that of a perfect network. An analogy can be made to a fishing net: knots on the net where strands meet signify hardeners, and connecting ropes symbolize epoxies. When the crosslinking is not at full capacity, the system resembles a net with gaps. Two nets with an equal count of missing knots (denoted by the same *CF*) might exhibit differing gap distributions: one could feature numerous small gaps scattered across (indicating a high S_{topo} value), while another might boast a solitary large gap (representing a low S_{topo} value). It is possible for a net with more absent knots (lower *CF*) to surpass another net in quality, provided it only has small gaps (high S_{topo}), in contrast to a net with a single substantial gap. A better network can be created by either increasing the *CF*, or by ensuring the topology of the network is the as close to perfect possible (i.e. the S_{topo} is high).

Interestingly, the f_3 systems do not follow the same trend as the rest. Specifically, a number of f_3 systems have relatively low-stress recoveries despite having intermediate topological scores. This can be explained as follows: During the preparation of the systems, we ensured that every hardener molecule that participates in the reaction has to form the maximum number of bonds possible. This means that in f_3 systems, a hardener

Table 1. Summary of the correlations between the fingerprints (H_f, E_2, F_{max}) and the stress recovery (σ_r). Statistically significant correlation coefficients (i.e. $p < 0.05$) are highlighted in green.

	Fingerprint	Coefficient	p-value
f_3	H_3	0.90	1.29×10^{-9}
	E_2	0.77	6.60×10^{-6}
	F_{max}	0.89	2.72×10^{-9}
	Fingerprint	Coefficient	p-value
f_4	H_4	0.46	0.02
	E_2	0.87	1.08×10^{-8}
	F_{max}	0.88	5.90×10^{-9}
	Fingerprint	Coefficient	p-value
f_5	H_5	0.43	0.03
	E_2	0.92	1.09×10^{-10}
	F_{max}	0.91	3.93×10^{-10}
	Fingerprint	Coefficient	p-value
f_6	H_6	0.54	0.006
	E_2	0.96	8.74×10^{-14}
	F_{max}	0.92	8.26×10^{-11}

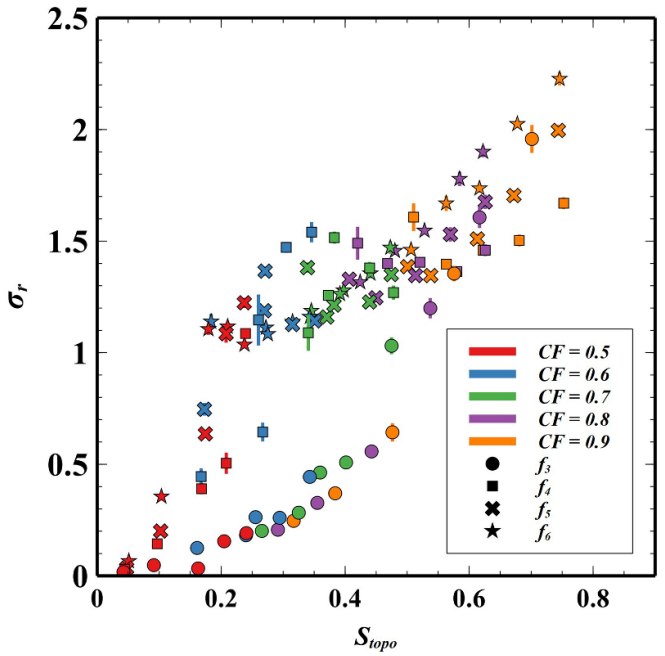

Figure 3. Plot of stress recovery (σ_r) vs. the topological score (S_{topo}) for f_3 (circle), f_4 (square), f_5 (cross) and f_6 (star) systems with different crosslinking fractions (CF) of 0.5 (red), 0.6 (blue), 0.7 (green), 0.8 (purple) and 0.9 (orange).

molecule will always have three bonds formed. These three bonds could either be between the hardener and three distinct epoxy molecules, or two distinct epoxy molecules. If the latter is true, then it means that a primary loop has formed (figure 4(a)). In this case, the hardener cannot contribute to network growth/extension. Thus, this specific configuration will act as a terminal point.

Such a terminal point contains a primary loop, which, as shown in our previous work [43], can adversely affect stress recovery. Moreover, the terminal point for an f_3 hardener can only be connected to the main network via one epoxy molecule, failing to expand the network. Consequently, these points cannot further expand the network and weaken its interconnectivity to a significant degree.

In our systems, an f_5 hardener can also form a terminal point (figure 4(b)) when it has formed five bonds but only with three distinct epoxies. While common in f_3 systems, these were relatively uncommon in f_5 systems because it requires two loops on the same hardener. On the other hand, in our systems, f_4 and f_6 hardeners, though they can form loops, cannot form terminal points. This is specific to the systematic method used to generate topologies. However, in a more realistic system where every hardener molecule has not necessarily formed the maximum number of possible bonds, f_4 and f_6 hardeners can also form terminal points. For example, an f_4 hardener that has formed three bonds with two of them making a primary loop (figure 4(c)) or an f_6 hardener that has formed two bonds with four of those forming two primary loops (figure 4(d)) can essentially form a terminal point.

To account for these kinds of defects, we adjust the topological scores of f_3 and f_5 systems by subtracting the number of molecules forming these terminal points (which would be three in this case: the hardener molecule, the two-distinctly reacted epoxy connecting the terminal point to the main network, and the one-distinctly reacted epoxy forming the loop) from the number of molecules that are part the main network, therefore adjusting F_{max}. Moreover, we subtract the two-distinctly reacted epoxy connecting the terminal point to the main network from the total number of two-distinctly reacted epoxies, thereby adjusting S_{topo}. The plot of stress recovery versus the adjusted topological score is shown in figure 5.

It can now be seen from figure 5 that the f_3 systems with adjusted topological scores follow the overall trend seen in other systems more closely. This behavior indicates the importance of taking into account the adverse effect of terminal points. In general, though, as the hardener functionality increases, the probability of forming a terminal point decrease. This is because more primary loops need to be formed before network expansion will be interrupted. For instance, for the f_5 hardeners, two primary loops would need to be formed to be in the same situation as the f_3 hardener with one primary loop.

Finally, it can be seen in both figures 3 and 5 that when comparing systems that have relatively similar topological scores but different f (i.e. number of functional groups per hardener molecule), those with a higher f usually have a higher stress recovery. Such a trend is more obvious for systems with a high topological score. All of the systems prepared for this study have the same number of total hardener molecules. When comparing systems that have the same CF and have close to perfect topology(i.e. $S_{topo} \sim CF^2$), those with a higher f have a higher reaction density (i.e. higher ratio of reactive to non-reactive beads), and we speculate that the higher reaction density leads to a higher recovery stress. Furthermore, the formation of primary loops is less detrimental to the overall properties of systems with a higher f (a single f_6 hardener can

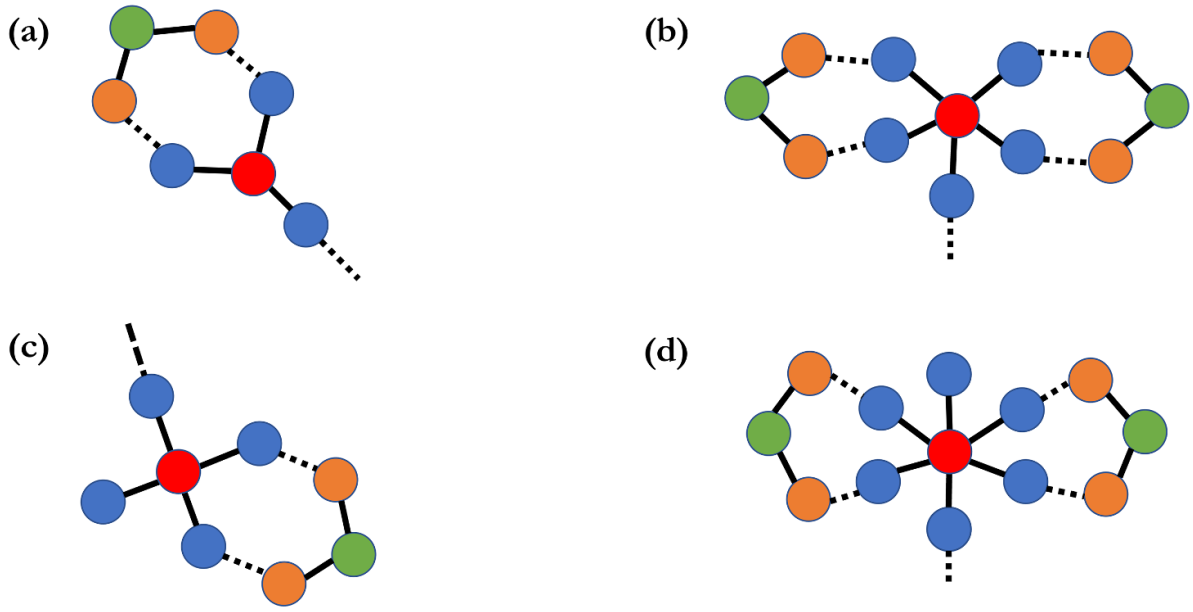

Figure 4. Schematic of terminal points formed by (a) hardener with three functional sites, (b) hardener with five functional sites, (c) hardener with four functional sites, and (d) hardener with six functional sites. The hardener molecules is represented blue and red beads, with the blue beads being the functional sites. The epoxy molecule is represented by the orange and green beads.

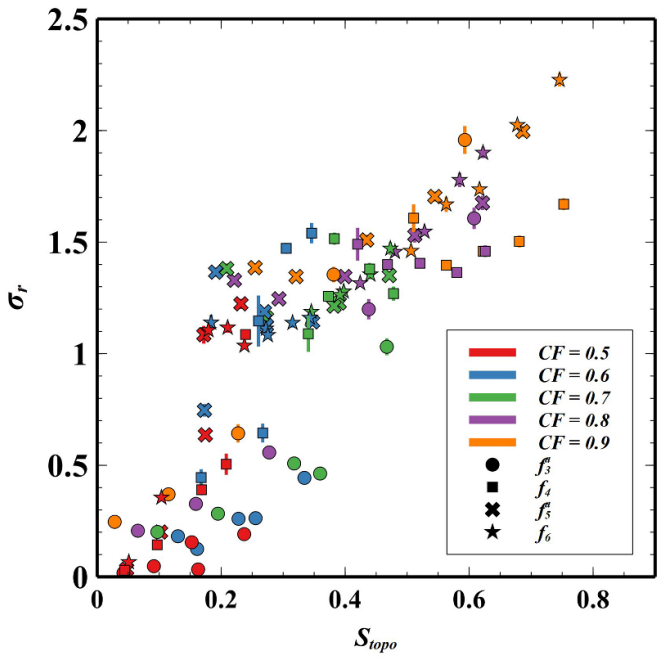

Figure 5. Plot of stress recovery (σ_r) vs. the topological score (S_{topo}) for f_3 (pentagons), f_4 (square), f_5 (cross) and f_6 (star) systems with different crosslinking fractions (CF) of 0.5 (red), 0.6 (blue), 0.7 (green), 0.8 (purple) and 0.9 (orange). The topological score for f_3 is system is adjusted.

have up two primary loops and still not be a terminal point while a single primary loop forming on an f_3 hardener turns it into a terminal point). While we have accounted for primary loops, higher order loops and defects are also possible, and we would expect higher functionality to mitigate the effect of those defects for the same reason.

It is evident that increasing f can lead to an increase in stress recovery, an effect that is more significant when S_{topo} is high One can conclude that increasing f, combined with techniques that aim to improve the topology of the network will lead to an improvement in stress recovery. Higher f can be achieved experimentally by adding amine groups to an amine-based hardener, while techniques like semi batch monomer addition [54], could increase the network quality and S_{topo}.

4. Conclusion

We studied the effect of crosslinking fraction and the number of functional sites per hardener molecule on the topology of the thermoset shape memory polymers, and consequently on their shape memory properties, via coarse-grained molecular dynamics simulations. We created a set of 100 systems with various crosslinking fractions ranging from 0.5 to 0.9 and a different number of functional groups per hardener molecule ranging from 3 to 6 and calculated their stress recovery. We defined three fingerprints used for quantifying the topological features of these networks: the fraction of hardener molecules that are connected to as many distinct epoxy molecules as possible (H_f), the fraction of epoxy molecules that are connected to two distinct hardener molecules (E_2), and the fraction of molecules that are part of the largest/main network in the system (F_{max}).

We observe that while all the correlations between H_f, E_2, F_{max}, and σ_r are statistically significant (i.e. their corresponding p-values is less than 0.05), the correlation coefficients corresponding to E_2 and F_{max} are significantly greater—and their p-values significantly smaller—than those corresponding to H_4, H_5, and H_6. We further improved upon this by defining the 'topological score' or S_{topo} that is defined by $S_{topo} = E_2 F_{max}$.

F_{max} scales the score by the number of molecules able to contribute to the network, and E_2 scales the score by the number of effective connections between those available molecules. We then further improved the effectiveness of this parameter by accounting for terminal hardeners within a network of odd-functional hardeners.

After analyzing the stress recovery as a function of the newly defined topological score, we found that:

- Systems with a lower crosslinking fraction can have a higher stress recovery than systems with a higher crosslinking fraction if they have a relatively high S_{topo}.
- When comparing systems with similar topological score, those with a higher f usually have a higher stress recovery.
- This phenomenon is more significant in systems with a relatively high topological score.

Our results confirm the possibility of achieving better shape memory properties via topology manipulation and suggest that a new approach that combines increasing the number of functional sites per hardener molecule (by, for example, adding an additional amine group to an amine-based hardener) with an approach that improves the topology of the network, such as semi batch monomer addition [54] (which has not yet been used to produce TSMPs), can result in production of TSMPs with superior shape memory properties.

Data availability statement

The data cannot be made publicly available upon publication because they are not available in a format that is sufficiently accessible or reusable by other researchers. The data that support the findings of this study are available upon reasonable request from the authors.

Acknowledgments

This study is funded by the US National Science Foundation under Grant Number OIA-1946231 and the Louisiana Board of Regents for the Louisiana Materials Design Alliance (LAMDA). The high-performance computing resources provided by the Louisiana Optical Network Infrastructure (LONI) were used to conduct all the simulations for this study.

ORCID iDs

Pouria Nourian https://orcid.org/0000-0001-5270-7639
Collin D Wick https://orcid.org/0000-0002-0261-0780
Andrew J Peters https://orcid.org/0000-0001-5031-2828

References

[1] Pilate F, Toncheva A, Dubois P and Raquez J-M 2016 Shape-memory polymers for multiple applications in the materials world *Eur. Polym. J.* **80** 268–94
[2] Lei M *et al* 2019 Recent progress in shape memory polymer composites: methods, properties, applications and prospects *Nanotechnol. Rev.* **8** 327–51
[3] Yakacki C M, Shandas R, Lanning C, Rech B, Eckstein A and Gall K 2007 Unconstrained recovery characterization of shape-memory polymer networks for cardiovascular applications *Biomaterials* **28** 2255–63
[4] El Feninat F, Laroche G, Fiset M and Mantovani D 2002 Shape memory materials for biomedical applications *Adv. Eng. Mater.* **4** 91–104
[5] Gall K, Yakacki C M, Liu Y, Shandas R, Willett N and Anseth K S 2005 Thermomechanics of the shape memory effect in polymers for biomedical applications *J. Biomed. Mater. Res.* A **73** 339–48
[6] Lendlein A and Kelch S 2005 Shape-memory polymers as stimuli-sensitive implant materials *Clin. Hemorheol. Microcirc.* **32** 105–16
[7] Lendlein A and Langer R 2002 Biodegradable, elastic shape-memory polymers for potential biomedical applications *Science* **296** 1673–6
[8] Metcalfe A, Desfaits A-C, Salazkin I, Yahia L, Sokolowski W M and Raymond J 2003 Cold hibernated elastic memory foams for endovascular interventions *Biomaterials* **24** 491–7
[9] Shmulewitz A, Langer R and Patton J 2006 Convergence in biomedical technology *Nat. Biotechnol.* **24** 277
[10] Wischke C, Schossig M and Lendlein A 2014 Shape-memory effect of micro-/nanoparticles from thermoplastic multiblock copolymers *Small* **10** 83–87
[11] Xiao Y, Zhou S, Wang L, Zheng X and Gong T 2010 Crosslinked poly (ε-caprolactone)/poly (sebacic anhydride) composites combining biodegradation, controlled drug release and shape memory effect *Composites* B **41** 537–42
[12] Lan X, Liu Y, Lv H, Wang X, Leng J and Du S 2009 Fiber reinforced shape-memory polymer composite and its application in a deployable hinge *Smart Mater. Struct.* **18** 024002
[13] Liu Y, Du H, Liu L and Leng J 2014 Shape memory polymers and their composites in aerospace applications: a review *Smart Mater. Struct.* **23** 023001
[14] Mao Y, Yu K, Isakov M S, Wu J, Dunn M L and Jerry Qi H 2015 Sequential self-folding structures by 3D printed digital shape memory polymers *Sci. Rep.* **5** 1–12
[15] Santo L, Quadrini F, Accettura A and Villadei W 2014 Shape memory composites for self-deployable structures in aerospace applications *Proc. Eng.* **88** 42–47
[16] Chen C M and Yang S 2014 Directed water shedding on high-aspect-ratio shape memory polymer micropillar arrays *Adv. Mater.* **26** 1283–8
[17] Fang Z *et al* 2017 Programmable shape recovery process of water-responsive shape-memory poly (vinyl alcohol) by wettability contrast strategy *ACS Appl. Mater. Interfaces* **9** 5495–502
[18] Li J, Shim J, Deng J, Overvelde J T B, Zhu X, Bertoldi K and Yang S 2012 Switching periodic membranes via pattern transformation and shape memory effect *Soft Matter* **8** 10322–8
[19] Wang Z, Hansen C, Ge Q, Maruf S H, Ahn D U, Qi H J and Ding Y 2011 Programmable, pattern-memorizing polymer surface *Adv. Mater.* **23** 3669–73
[20] Fan J and Li G 2018 High enthalpy storage thermoset network with giant stress and energy output in rubbery state *Nat. Commun.* **9** 642
[21] Ivens J 2011 Shape recovery in a thermoset shape memory polymer and its fabric-reinforced composites *Express Polym. Lett.* **5** 254–61

[22] Ni Q-Q, Zhang C-S, Fu Y, Dai G and Kimura T 2007 Shape memory effect and mechanical properties of carbon nanotube/shape memory polymer nanocomposites *Compos. Struct.* **81** 176–84

[23] Koerner H, Price G, Pearce N A, Alexander M and Vaia R A 2004 Remotely actuated polymer nanocomposites—stress-recovery of carbon-nanotube-filled thermoplastic elastomers *Nat. Mater.* **3** 115–20

[24] Meng Q and Hu J 2009 A review of shape memory polymer composites and blends *Composites* A **40** 1661–72

[25] Gunes I S, Cao F and Jana S C 2008 Evaluation of nanoparticulate fillers for development of shape memory polyurethane nanocomposites *Polymer* **49** 2223–34

[26] Gall K *et al* 2002 Shape memory polymer nanocomposites *Acta Mater.* **50** 5115–26

[27] Zhang C-S and Ni Q-Q 2007 Bending behavior of shape memory polymer based laminates *Compos. Struct.* **78** 153–61

[28] Gall K, Mikulas M, Munshi N A, Beavers F and Tupper M 2000 Carbon fiber reinforced shape memory polymer composites *J. Intell. Mater. Syst. Struct.* **11** 877–86

[29] Elliott J E, Nie J and Bowman C N 2003 The effect of primary cyclization on free radical polymerization kinetics: experimental characterization *Polymer* **44** 327–32

[30] Elliott J E and Bowman C N 2002 Effect of primary cyclization on free radical polymerization kinetics: modeling approach *Macromolecules* **35** 7125–31

[31] Odian G 2004 *Principles of Polymerization* (Wiley)

[32] Syed I H, Stratmann P, Hempel G, Klüppel M and Saalwächter K 2016 Entanglements, defects, and inhomogeneities in nitrile butadiene rubbers: macroscopic versus microscopic properties *Macromolecules* **49** 9004–16

[33] Metters A and Hubbell J 2005 Network formation and degradation behavior of hydrogels formed by Michael-type addition reactions *Biomacromolecules* **6** 290–301

[34] Elliott J E, Macdonald M, Nie J and Bowman C N 2004 Structure and swelling of poly(acrylic acid) hydrogels: effect of pH, ionic strength, and dilution on the crosslinked polymer structure *Polymer* **45** 1503–10

[35] Vorov O K, Livesay D R and Jacobs D J 2008 Conformational entropy of an ideal cross-linking polymer chain *Entropy* **10** 285–308

[36] Reneker D H, Kataphinan W, Theron A, Zussman E and Yarin A L 2002 Nanofiber garlands of polycaprolactone by electrospinning *Polymer* **43** 6785–94

[37] Beshah K, Mark J E and Ackerman jJ L 1986 Topology of poly(dimethylsiloxane) elastomeric networks studied by variable-temperature solid-state nuclear magnetic resonance *Macromolecules* **19** 2194–6

[38] Wang J, Lin T-S, Gu Y, Wang R, Olsen B D and Johnson J A 2018 Counting secondary loops is required for accurate prediction of end-linked polymer network elasticity *ACS Macro Lett.* **7** 244–9

[39] Wang R, Alexander-Katz A, Johnson J A and Olsen B D 2016 Universal cyclic topology in polymer networks *Phys. Rev. Lett.* **116** 188302

[40] Lin T-S, Wang R, Johnson J A and Olsen B D 2018 Topological structure of networks formed from symmetric four-arm precursors *Macromolecules* **51** 1224–31

[41] Akagi Y, Gong J P, Chung U-I and Sakai T 2013 Transition between phantom and affine network model observed in polymer gels with controlled network structure *Macromolecules* **46** 1035–40

[42] Zhong M, Wang R, Kawamoto K, Olsen B D and Johnson J A 2016 Quantifying the impact of molecular defects on polymer network elasticity *Science* **353** 1264–8

[43] Nourian P, Wick C D, Li G and Peters A J 2022 Correlation between cyclic topology and shape memory properties of an amine-based thermoset shape memory polymer: a coarse-grained molecular dynamics study *Smart Mater. Struct.* **31** 105014

[44] Shafe A, Wick C D, Peters A J, Liu X and Li G 2022 Effect of atomistic fingerprints on thermomechanical properties of epoxy-diamine thermoset shape memory polymers *Polymer* **242** 124577

[45] Weeks J D, Chandler D and Andersen H C 1971 Role of repulsive forces in determining the equilibrium structure of simple liquids *J. Chem. Phys.* **54** 5237–47

[46] Kremer K and Grest G S 1990 Dynamics of entangled linear polymer melts: a molecular-dynamics simulation *J. Chem. Phys.* **92** 5057–86

[47] Sliozberg Y R, Chantawansri T L, Lenhart J L and Andzelm J W 2014 Structural and mechanical properties of advanced polymer gels with rigid side-chains using coarse-grained molecular dynamics *Polymer* **55** 5266–75

[48] Sliozberg Y R *et al* 2013 Effect of polymer solvent on the mechanical properties of entangled polymer gels: coarse-grained molecular simulation *Polymer* **54** 2555–64

[49] Wang J and Shi X 2017 Molecular dynamics simulation of diffusion of nanoparticles in mucus *Acta Mech. Solida Sin.* **30** 241–7

[50] Plimpton S 1995 Fast parallel algorithms for short-range molecular dynamics *J. Comput. Phys.* **117** 1–19

[51] Nosé S 1984 A unified formulation of the constant temperature molecular dynamics methods *J. Chem. Phys.* **81** 511–9

[52] Shinoda W, Shiga M and Mikami M 2004 Rapid estimation of elastic constants by molecular dynamics simulation under constant stress *Phys. Rev.* B **69** 134103

[53] Abbott L J, Hart K E and Colina C M 2013 Polymatic: a generalized simulated polymerization algorithm for amorphous polymers *Theor. Chem. Acc.* **132** 1334

[54] Gu Y, Kawamoto K, Zhong M, Chen M, Hore M J A, Jordan A M, Korley L T J, Olsen B D and Johnson J A 2017 Semibatch monomer addition as a general method to tune and enhance the mechanics of polymer networks via loop-defect control *Proc. Natl Acad. Sci.* **114** 4875–80